Inorganic Chemistry

Article

pubs.acs.org/IC

The Cu^{2+} Binding Properties of Branched Peptides Based on L-2,3-Diaminopropionic Acid

Łukasz Szyrwiel,*[,†] Łukasz Szczukowski,[‡] József S. Pap,[§] Bartosz Setner,[∥] Zbigniew Szewczuk,[∥] and Wiesław Malinka[‡]

[†]CNRS/UPPA, LCABIE, UMR5254, Hélioparc, 2, av. Pr. Angot, F-64053 Pau, France

[‡]Department of Chemistry of Drugs, Wrocław Medical University, ul. Borowska 211, 50-552 Wrocław, Poland

[§]Surface Chemistry and Catalysis Department, Centre for Energy Research, Hungarian Academy of Sciences, 1525 Budapest 114, P.O. Box 49, Budapest, Hungary

[∥]Faculty of Chemistry, University of Wrocław, ul. F. Joliot-Curie 14, 50−383 Wrocław, Poland

Supporting Information

ABSTRACT: Three new branched peptides, namely, H-Gly-Dap(H-Gly)-Gly-NH_2 (3G), H-His-Dap(H-His)-Gly-NH_2 (2HG), and H-Gly-Dap(H-Gly)-His-NH_2 (2GH), where Dap stands for the 2,3-diaminopropionic acid residue, were synthesized by solid phase procedures. Because of the junction at Dap these peptides have three available pending arms for metal chelation. The complex formation between these peptides and 1 equiv of Cu^{2+} was investigated as a function of pH by potentiometry ultraviolet−visible absorption, circular dichroism, and X-band electron paramagnetic resonance spectroscopy in aqueous medium. Our results clearly demonstrate that cooperation between all three peptide arms essentially contributes to the stability of copper(II) complexes.

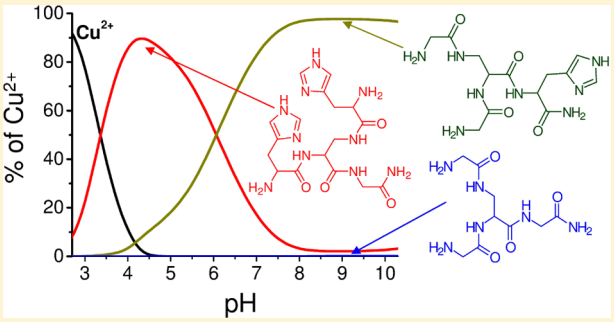

INTRODUCTION

Branched peptides are highly variable through their pending arms, which makes them attractive models for studying various biological activities,[1,2] for example, antibacterial, immunological,[3] gene transfer,[4] enzyme-like,[5,6] associations with receptors,[2] and selective targeting.[7] In addition, these peptides may serve as junction points for dendrimers designed for catalytic purposes with activity gained by the formation of Cu^{2+} peptide complexes. Especially interesting examples are those that exhibit unusual protease resistance[8] or unusual activity toward metal chelation in biological systems.[9]

In the present work we focus on three *de novo* branched peptides based on the L-2,3-diaminopropionic acid (Dap). Designed peptides compared to linear analogues in their structure contain an additional N-terminal residue, which could be effective in stabilization of copper binding.[10−12]

We report the synthesis and characterization of three new peptides H-Gly-Dap(H-Gly)-Gly-NH_2 (3G), H-His-Dap(H-His)-Gly-NH_2 (2HG), and H-Gly-Dap(H-Gly)-His-NH_2 (2GH) (Figure 1), and the systematic spectroscopic (UV−vis), electron paramagnetic resonance (EPR), circular dichroism (CD), potentiometric, and electrospray ionization mass spectrometry (ESI-MS) studies on their complexes with 1 equiv of Cu^{2+} as a function of pH. The ligand 3G was designed to elucidate the role of the peptide backbone in the coordination of Cu^{2+}. Further comparison with 2HG will provide answers about the impact of N-terminal histidine residues on the binding of Cu^{2+}. The effect of the localization of histidine at the C-terminal residue was examined through the 2GH branch peptide.

EXPERIMENTAL SECTION

Peptide Synthesis. The syntheses were performed manually on Rink Amide MBHA resin (loading: 0.52×10^{-3} M/g) in a polypropylene syringe reactor (Intavis AG, Köln, Germany) equipped with polyethylene filter, according to the Fmoc (9-fluorenylmethoxycarbonyl) solid phase synthesis procedure as described by us previously for peptides branched on lysine residue.[13] *O*-(Benzotriazol-1-yl)-*N*,*N*,*N*′,*N*′-tetramethyluronium tetrafluoroborate (TBTU) was used as a coupling reagent. Ethyl 2-cyano-2-(hydroxyimino)-acetate (Oxyma Pure) and *N*,*N*-diisopropylethylamine (DIPEA) were used as additives. *N*,*N*-Dimethylformamide (DMF) was used as solvent. All Fmoc amino acids, including Fmoc-L-Dap(Fmoc)−OH, and reagents were purchased from Iris Biotech GmbH and used as received. Each coupling step was performed for 2 h except the final step, which was performed for 24 h. The end of each coupling reaction was confirmed by Kaiser Test. Peptides were cleaved from the resin simultaneously with the side chain deprotection using a solution of trifluoroacetic acid and triisopropylsilane (TFA)/H_2O/TIS (95/2.5/2.5, v/v/v) at room temperature for 2 h. The peptides were purified by the high-performance liquid chromatography (HPLC) using a Varian

Received: April 1, 2014
Published: July 14, 2014

   dx.doi.org/10.1021/ic5007428 | *Inorg. Chem.* 2014, 53, 7951−7959

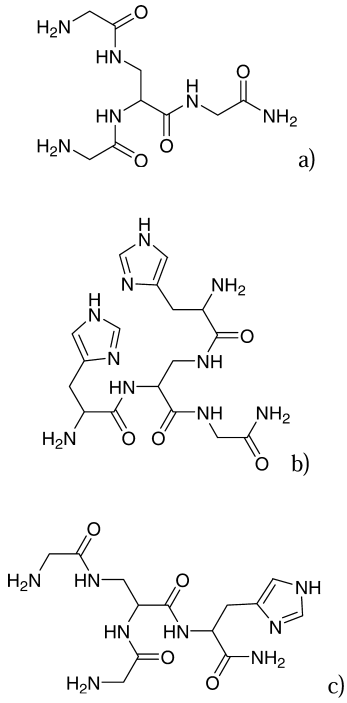

Figure 1. Structural formula of the investigated ligands (a) 3G (H-Gly-Dap(H-Gly)-Gly-NH_2), (b) 2HG (H-His-Dap(H-His)-Gly-NH_2), and (c) 2GH (H-Gly-Dap(HGly)-His-NH_2). Within the text these ligands in general are referred to as H*x*L (where $x = -3, -2, -1, 0, 1,$ or 2).

ProStar (Palo Alto, CA) with UV detection (210 nm) on a TSKgel ODS-120T column (215 × 30.0 mm, 10 μm) equipped with a guard column, with a gradient elution of 0−80% B in A (A = 0.1% TFA in water; B = 0.1% TFA in acetonitrile/H_2O, 4:1) for 40 min (flow rate = 7 mL/min). The main peak, corresponding to the desired product, was collected, and the fraction was lyophilized. The purified ligands were obtained as trifluoroacetate salts. Their purity was determined by potentiometric titrations, and their molecular weight was confirmed by ESI-MS. The m/z obtained for $[M + H]^+$ ions of H-His-Dap(H-His)-Gly-NH_2, HGly-Dap(H-Gly)-Gly-NH_2, and H-Gly-Dap(H-Gly)-His-NH_2 were 435.2225 (calculated 435.2229), 275.1462 (calculated 275.1463) and 355.1836 (calculated 355.1836), respectively.

Potentiometric Studies. Peptide protonation and Cu^{2+} complex stability constants were calculated from three titration curves carried out over the pH range of 2.5−11.0 at 298 K under argon atmosphere. Ligand concentration was set in the range from 1×10^{-3} to 1.5×10^{-3} M. Metal-to-ligand ratio was up to 0.95:1. The pH-metric titrations were performed in 0.1 M KCl on a Metrohm titrator using a Mettler Toledo InLabMicro combined electrode calibrated for hydrogen ion concentration using HCl. The stability constants were calculated with HYPERQUAD 2013 program from three titrations for each investigated system.[14] Standard deviations quoted were computed with the same software and refer to random errors only.

Spectroscopic Studies (UV−vis, CD, EPR). Absorption spectra of Cu^{2+} complexes were recorded on a PerkinElmer Lambda 25 spectrophotometer in 1 and 0.5 cm path length quartz cells. All UV−vis spectra were collected in the 300−900 nm range.

Circular dichroism (CD) spectra were recorded on a JASCO J 750 spectropolarimeter in the 250−900 nm range, using 1 and 0.1 cm cuvettes. Spectroscopic measurements were carried out at 298 K, at concentrations from 0.8 to 1.4×10^{-3} M and M/L = 1:1.

Electron paramagnetic resonance (EPR) spectra were measured on a Bruker ESP 300E instrument at X-band frequency (9.4 GHz) at liquid nitrogen temperature using narrow quartz capillaries to reduce the dielectric loss of the cavity. The ligand concentration was adjusted to $(1-1.5) \times 10^{-3}$ M in 30% (v/v) polyethylene glycol/water solution. Data from X-Band EPR spectroscopy were extracted by simulation of the experimental spectra taken at different pH values, at 123 K. The anisotropic g values and the A^{Cu} hyperfine (hf) and a^N superhyperfine (shf) couplings listed in Tables 2−4 were determined by using the WIN95EPR software,[15] which is suitable for handling spin mixtures. Before starting the simulations the results from potentiometric titrations and from UV−vis and CD spectroscopies were considered to estimate the contributions from the different $Cu_xH_yL_z$ macrospecies to the total spin concentration at the given pH values. Potentiometric data were considered to find the pH values where the major species were present in at least 95% abundance. Parameters from such spectra provided the starting point for refining further simulations. Simulations were preformed by fixing the $g_\parallel$ and $A_\parallel^{Cu}$ values, which could be read from the experimental data, and sequential fitting of the g_x and g_y values along with the corresponding A^{Cu}, a^N, and line broadening values by the Monte Carlo method of the software. Simulations were restricted to Lorentzian curves, and the coupling of the unpaired electron to the ^{63}Cu (69%, $I = 3/2$) and ^{65}Cu (31%, $I = 3/2$) isotopes was included. In concomitant rounds all three anisotropic parameters were fitted again sequentially with step-by-step smaller allowance until no further improvement was achieved. The software uses the total double integral and its variance (square of the standard deviation, σ^2) for fitting. The spectral fit was characterized by the average standard deviation (e.g., the square root of σ^2 divided by the number of spectral points, 1024), which was between 0.18 and 1.16% for all the simulations expressed in % of the total double integral of the simulated spectrum relative to the total double integral of the experimental spectrum. The concentration of each species was related to the overall concentration of EPR-active species. The parameters from these "neat" spectra were used for the simulation of spin mixtures and the parameters for those $Cu_xH_yL_z$ species, which are present only mixed with other species were determined according to the above algorithm. Omitting any of the included species (e.g., component spectrum) significantly decreases the goodness of the fit. Figures S1 and S6 show the measured spectra (in red) and the simulated ones (in black) for the 3G, 2HG and 2GH containing solution of Cu^{2+} at 1:1 molar ratio, respectively.

Mass Spectrometry Measurements. High-resolution mass spectra were obtained on a Bruker micrOTOF-Q mass spectrometer. ESI-MS mass spectra were measured in the positive ion mode. Before each run the instrument was calibrated externally with the Tunemix mixture. The ion source parameters were as follows: dry gas−nitrogen, temperature 170 °C, transfer time 120 ps, collision voltage −1.0 EV. The sample was dissolved in aqueous solution, while the pH was adjusted with ammonium acetate to 4.5 and 6.8 and with ammonium carbonate to 9.5. The peptide concentration was in the $10^{-5}-10^{-4}$ M range. The solution was infused at a flow rate of 3 μL/min. Simulations of the isotopic patterns were calculated using BrukerDataAnalysis 4.0 software.

RESULTS

Ligand 3G. This ligand consists of three glycyl units attached by peptide bonds to the "central" Dap fragment (Figure 1a). The protonation and stability constants of Cu^{2+} complexes with the investigated ligands are presented in Table 1. The speciation diagram for the 3G complexes is presented in Figure 2a. The potentiometric results and changes in spectroscopic behavior (Tables 1 and 2, Figures 3a, 4a, and in the Supporting Information, Figure S1a) indicate complex formation with 3G when pH is increased from 4.5 to 7.0. In this range of pH the observed species could be assigned as $Cu_2H_{-1}L_2$, $CuH_{-1}L$, and $CuH_{-2}L$ with increasing pH. The simultaneous presence of $Cu_2H_{-1}L_2$ and $CuH_{-1}L$ in equilibrium with two other Cu^{2+} forms (Cu^{2+}_{aq}, and $CuH_{-2}L$) do not allow for a precise definition of the coordination sphere for the $Cu_2H_{-1}L_2$ and $CuH_{-1}L$ forms (Figure 2a). However, the EPR spectroscopic results (Table 2 and Supporting Information, Figure S1a) support the occurrence of two additional species to

dx.doi.org/10.1021/ic5007428 | Inorg. Chem. 2014, 53, 7951−7959

Table 1. Logarithms of the Protonation Constants ($\log \beta_{HxL}$) and Stability Constants ($\log \beta_{CuxHyLz}$) for Copper(II) Complexes; UV−vis and CD Spectroscopic Data for the Proposed Complexes with 3G, 2HG, and 2GH (T = 298 K, I = 0.1 M KCl)

	3G				2HG				2GH			
			UV−vis	CD			UV−vis	CD			UV−vis	CD
	$\log \beta$	$\log K$	(λ [nm], ε [M^{-1} cm^{-1}])	(λ [nm], $\Delta\varepsilon$ [M^{-1} cm^{-1}])	$\log \beta$	$\log K$	(λ [nm], ε [M^{-1} cm^{-1}])	(λ [nm], $\Delta\varepsilon$ [M^{-1} cm^{-1}])	$\log \beta$	$\log K$	(λ [nm], ε [M^{-1} cm^{-1}])	(λ [nm], $\Delta\varepsilon$ [M^{-1} cm^{-1}])
H_4L					24.92(2)	4.55						
H_3L					20.37(2)	5.57			21.63(3)	6.08		
H_2L	15.55(1)	7.35			14.80(1)	6.89			15.55(2)	7.36		
HL	8.20(1)				7.91(2)				8.19(2)			
CuH_2L					21.50(1)		684, 46	682^a, 0.17				
$Cu_2H_2L_2$					37.71(5)							
CuHL									15.85(5)			
CuL					12.98(1)		620, 100	668^a, 0.74 321^c, −0.41				
$Cu_2H_{-1}L_2$	13.96(2)											
$CuH_{-1}L$	2.56(2)	6.67							7.80(1)		529, 98	568^a, −0.58 481^a, 0.23 305^b, 1.08 270^c, −2.05
$CuH_{-2}L$	−4.11(1)	10.69	528, 155	549^a, 0.09 468^a, −0.14 296^b, −0.87 250^d, sh	−3.13(2)	10.12	528, 178	545^a, 0.60 461^a, −0.18 303^b, −0.92 261^c, sh	−0.21(5)	8.01	528, 101	569^a, −0.57 480^a, 0.22 305^b, 1.08 270^c, −2.05
$CuH_{-3}L$	−14.80(2)		526, 122	545^a, 0.02 469^a, −0.18 295^b, −0,41 250^d, sh	−13.26(2)		524, 120	546^a, 0.59 459^a, −0.11 303^b, −0.86 257^c, sh				

[a] d−d transition. [b] $N^- \rightarrow Cu(II)$ charge transfer (CT) transition. [c] $N_{Im} \rightarrow Cu(II)$ CT transition. [d] $NH_2 \rightarrow Cu(II)$ CT transition.

dx.doi.org/10.1021/ic5007428 | Inorg. Chem. 2014, 53, 7951−7959

Table 2. EPR Simulation Parameters for the pH-Dependent Cu-3G Species and Cu^{2+}[a]

	Cu^{2+}	$Cu_2H_{-1}L_2$[b]	$CuH_{-1}L$	$CuH_{-2}L$	$CuH_{-3}L$
$g_\parallel$ (g_z)	2.4158	2.3910 2.2308	2.1965	2.1896	2.1816
$g_\perp$ (g_x, g_y)	2.0835	2.0629, 2.0861 2.0472, 2.0683	2.0405, 2.0572	2.0392, 2.0449	2.0374, 2.0415
$A_\parallel^{Cu}$ (A_z^{Cu})	128	140 160	186	196	193
$A_\perp^{Cu}$ (A_x^{Cu}, A_y^{Cu})	4	22, 25 9, 20	10, 12	19, 29	11, 21
$a_\parallel^{Nc}$		8 (2N) 8 (3N)	8 (3N)	7 (4N)	8 (4N)
$a_\perp^{N}$		9, 9 (2N) 12, 13 (3N)	11, 13 (3N)	13, 14 (4N)	12, 13 (4N)

[a] $[|A|] = 10^{-4}$ cm^{-1}. [b] Two noncoupled Cu centers were considered. [c] Estimation from unresolved structures (the effect is comparable to line broadening).

Table 3. EPR Simulation Parameters for the pH-Dependent Cu-2HG Species and Cu^{2+}[a]

	Cu^{2+}	CuH_2L	CuL	$CuH_{-2}L$	$CuH_{-3}L$
$g_\parallel$ (g_z)	2.4167	2.3049	2.2388	2.1874	2.1868
$g_\perp$ (g_x, g_y)	2.0803	2.0687	2.0459, 2.0718	2.0412, 2.0540	2.0394, 2.0471
$A_\parallel^{Cu}$ (A_z^{Cu})	126	162	178	195	194
$A_\perp^{Cu}$ (A_x^{Cu}, A_y^{Cu})	4	12	18, 23	19, 27	21, 23
$a_\parallel^{N}$[b]		13 (2N)	10 (3N)	7 (4N)	8 (4N)
$a_\perp^{N}$		7 (2N)	14, 13 (3N)	9, 13 (4N)	11, 13 (4N)

[a] $[|A|] = 10^{-4}$ cm^{-1}. [b] Estimation from unresolved structures (the effect is comparable to line broadening).

Table 4. EPR Simulation Parameters for the pH-Dependent Cu-2GH Species and Cu^{2+}[a]

	Cu^{2+}	$CuHL$[b]	$CuH_{-1}L$	$CuH_{-2}L$
$g_\parallel$ (g_z)	2.4154	2.2367	2.1896	2.1884
$g_\perp$ (g_x, g_y)	2.0825	2.0746	2.0390, 2.0496	2.0397, 2.0498
$A_\parallel^{Cu}$ (A_z^{Cu})	127	158	194	191
$A_\perp^{Cu}$ (A_x^{Cu}, A_y^{Cu})	4	12	12, 21	13, 19
$a_\parallel^{Nc}$		8 (2N)	8 (4N)	9 (4N)
$a_\perp^{N}$		10 (2N)	12, 14 (4N)	9, 13 (4N)

[a] $[|A|] = 10^{-4}$ cm^{-1}. [b] Parameters are estimated values due to the very low proportion of this species. [c] Estimation from unresolved structures (the effect is comparable to line broadening).

Cu_{aq}^{2+} and $CuH_{-2}L$ in this pH range with the presence of two and/or three N donor atoms in the equatorial plane of the coordination polyhedron (see Table 2 for data). The observed axial-type spectra with $g_z > (g_x + g_y)/2 > 2.04$ (slight rhombic distortion is experienced) are typical for $d_{x^2-y^2}$ ground state[16] that in turn supports a "classic" elongated square-(bi)pyramidal geometry (*vide infra*). The presence of dinuclear forms (2Cu/2L) is often reported in the literature; for example, the 2Cu/2L is the dominant species between pH 4 and 7 in the case of *N,N′*-diglycylethane-1,2-diamine (DGEN)[17] or *N,N′*-dialanylethane-1,2-diamine (DAEN)[18] (Supporting Information, Figure S2a,b). The DGEN-like domain of 3G (Figure S2c) is the responsible fragment for interactions with Cu^{2+} (presented in Discussion). The dimeric form is only a minor species in the Cu-3G system between pH 5 and 7, unlike the case of DGEN[17,19] or DAEN.[18] This difference is a result of the branched ligand topology and the increased stability of the $CuH_{-2}L$ complex at lower pH[18] (presented in Discussion). In the case of $CuH_{-1}L$ complex the 3N coordination sphere could be proposed $\{2NH_2, N^-\}$ (Supporting Information, Figure S3). The latter form, $CuH_{-2}L$, becomes the dominant species above pH 7. All spectroscopic parameters (Tables 1 and 2, Supporting Information, Figure S1a) support that copper is bound by four N donor atoms in the equatorial plane, $\{2NH_2, 2N^-\}$ (Figure 5), which is in reasonable agreement with the data for the DGEN ligand.[17] The lack of any other acidic protons in the 3G peptide allows the conclusion that the occurrence of a deprotonation step resulting in $CuH_{-3}L$ is related to the proton loss from an axially coordinated water molecule when pH is increased from 9 to 11. The deprotonation of axial water between pH 9.85 and 11.15 has been demonstrated earlier in the literature.[20]

It is apparent from the experimental X-band EPR spectra that the $S = 1/2$ species give axial signals with $g_\parallel > g_\perp > 2.0$. The characteristic $A_\parallel^{Cu} \gg A_\perp^{Cu}$ splitting pattern is typical for $d_{x^2-y^2}$ ground state.[16] However, minor rhombic anisotropy occurs at higher pH values. The simulated component spectra for the contributing species at a given pH were fitted by optimalization of the typical couplings of the unpaired electron to the ^{63}Cu and ^{65}Cu nuclei ($I = 3/2$). Superhyperfine (shf) coupling to nitrogen nuclei (^{14}N, $I = 1$) can be expected for the copper-peptide complexes. Although the shf couplings to different numbers of either equal or unequal nitrogen nuclei (Tables 2−4) in the equatorial positions often remain unresolved, they

dx.doi.org/10.1021/ic5007428 | Inorg. Chem. 2014, 53, 7951−7959

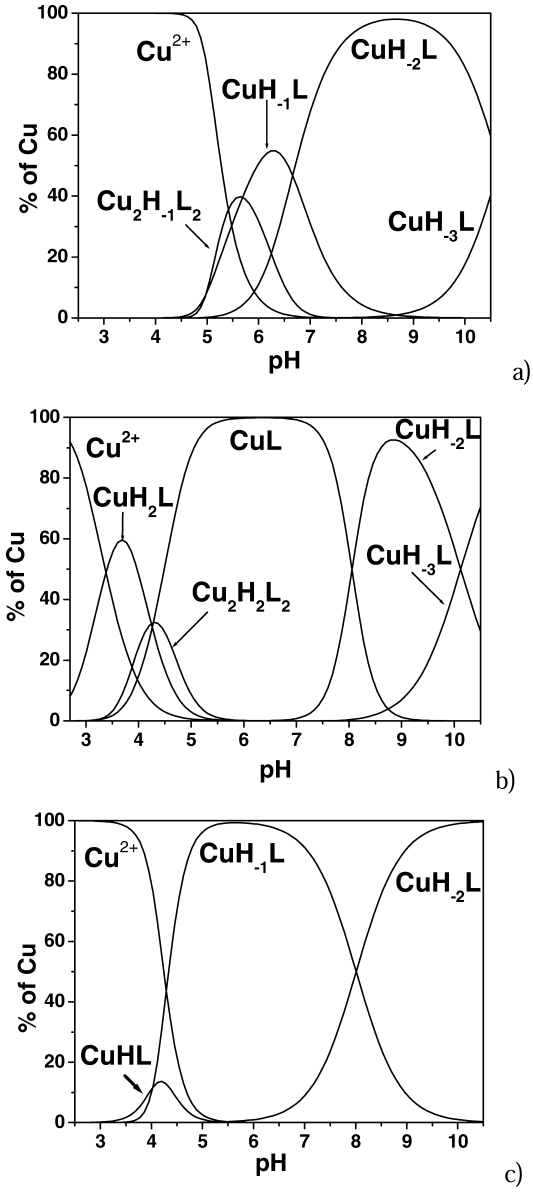

Figure 2. Speciation diagrams for the systems containing Cu^{2+} and the (a) 3G, (b) 2HG, and (c) 2GH peptide, $[Cu^{2+}] = 1 \times 10^{-3}$ M, 1:1 M/L ratio.

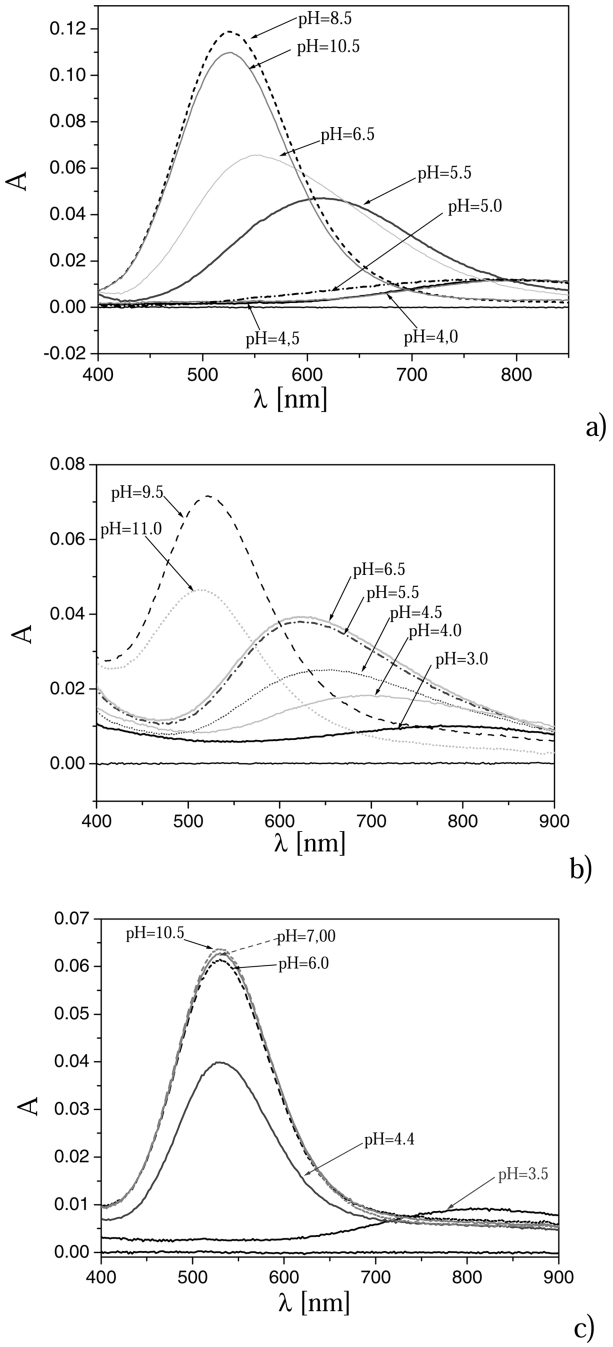

Figure 3. UV–vis spectral changes as a function of pH for Cu^{2+} in the presence of (a) 3G, (b) 2HG, and (c) 2GH in 0.9:1 M/L molar ratio (the $[Cu^{2+}] = 0.8 \times 10^{-3}$ M for 2HG, 1.4×10^{-3} M for 3G, and 1.2×10^{-3} M for 2GH system).

still contribute to the improvement of the fittings. Where rhombic g tensors of $g_z \gg g_y > g_x > 2.0$ are present the elongated octahedral (or square-based pyramidal) geometry that is indicated by the very low (<0.3) R values $[R = (g_y - g_x)/(g_z - g_y)]$[21] is further distorted.

Ligand 2HG. For the N-terminal histidine analogue of 3G, that is 2HG, the distribution of complexes as a function of pH is presented in Figure 2b. At pH 3.8 the Cu^{2+} is mainly bound in the CuH_2L form. The value of the corrected log $\beta^*_{CuH2L\text{-}H2L}$ = 6.75 is close to the log β^* found for the $\{2N_{Im}\}$ binding mode (log β^* = 6.41[22]) or log β for $\{2N_{Im}\}$ complex with peptide (log β_{CuL} = 6.48[23]). These data support that 2HG coordinates Cu^{2+} by two imidazole nitrogen donors in the CuH_2L species (Figure 6a). Both the UV–vis and EPR parameters presented in Tables 1 and 3 are in good agreement with those reported for macrochelates with two imidazole donors $\{2N_{Im}\}$.[23]

An attempt to elucidate the spectroscopic parameters for $Cu_2H_2L_2$ with the applied tools in this study was impeded by its low relative concentration and co-occurrence with other species at the investigated pH values. The presence of a relatively minor amount of dimer (when compared to the monomeric complexes) was confirmed from the ESI-MS spectra (Supporting Information, Figure S4a,b) at pH 4.5.

Above pH 5.5 the deprotonation of CuH_2L leads to CuL, which is predominantly present up to pH 8. This process is thought to occur through the intermediate form of $Cu_2H_2L_2$. The 1:1 Cu/2HG stoichiometry for CuL was confirmed by the ESI-MS spectra at two pH values: 6.8 and 9.5 (Supporting

dx.doi.org/10.1021/ic5007428 | Inorg. Chem. 2014, 53, 7951–7959

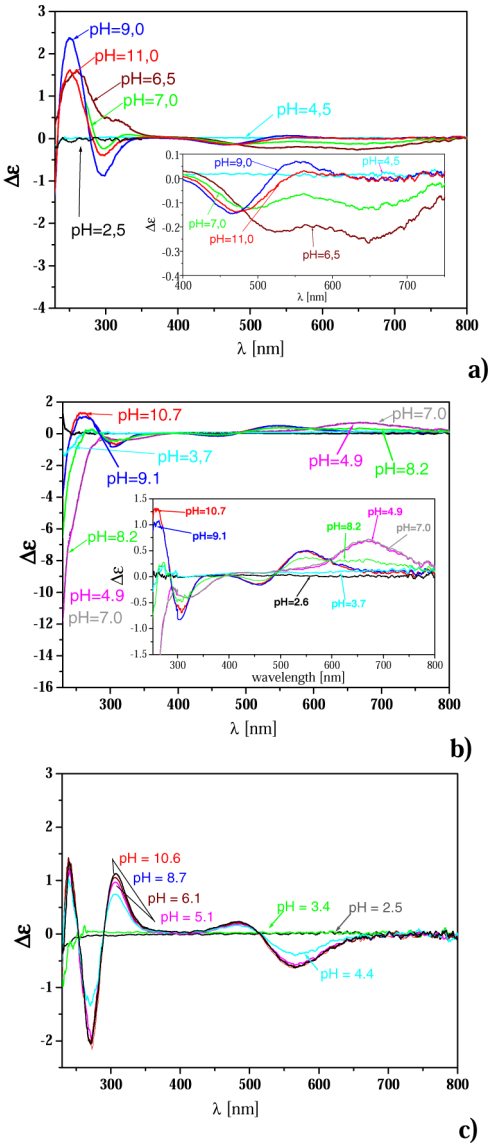

Figure 4. CD spectra of systems containing Cu^{2+} and the (a) 3G, (b) 2HG, (c) 2GH, ($[Cu^{2+}]$ = 1.4 × 10^{-3} M for 3G, 0.8 × 10^{-3} M for 2HG, 1.0 × 10^{-3} M for 2GH system, the metal to ligand ratio is 0.9:1).

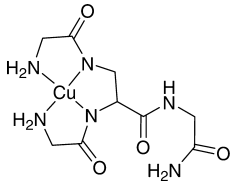

Figure 5. Proposed structure for major complex form ($CuH_{-2}L$) observed in the Cu^{2+}-3G system.

Information, Figure S5a,b[24]). The optical spectroscopy parameters, the changes in log *K* for the N-terminal amino groups (Table 1), and EPR parameters (Table 3 and Supporting Information, Figure S1b) for CuL all support that in this species Cu^{2+} is bound by three nitrogen donors in {$1N_{Im}$, $2NH_2$} donor set[25] (Figure 6b). Further changes with increasing the pH to 9 can be associated with the formation of a $CuH_{-2}L$ complex (Table 1). This is in line with literature findings, for example, with those for *N,N′*-dihistidylethane-1,2-diamine complexes.[26] In this case the double deprotonation step of Cu_2L_2 results in $Cu_2L_2H_{-4}$. Other examples clearly demonstrate that modifications in the ethane moiety of *N,N′*-XX-ethane-1,2-diamine (where XX = dialanyl, diglycyl, diphenylalanyl) lead to the increased stability of the $CuH_{-2}L$ form and direct double deprotonation of CuL to yield $CuH_{-2}L$.[18]

The EPR spectroscopic features of $CuH_{-2}L$ (Table 3 and Supporting Information, Figure S1b) and also the changes in CD spectroscopy (Figure 4b) all emerge in parallel confirming changes in the donor environment around the Cu^{2+} ion to the 4N {$2NH_2$, $2N^-$} (Figure 6c). The weak interactions with the imidazole nitrogen could be also observed from CD spectroscopy (Figure 4a,b), similar to the case of $CuH_{-2}L$ complexes with HisXaaXaa linear tripeptides, when compared to XaaXaaXaa (Xaa = Gly or Ala).[27]

The increase of pH to 11 results in $CuH_{-3}L$, most likely due to the deprotonation of a coordinated water molecule. In the case of lysine-based branched peptides the hydroxido form is proposed at the even lower p*K* value of 9.6.[9]

Ligand 2GH. In this peptide the C-terminal glycyl residue of 3G was replaced by a histidyl residue (Figure 1c). This modification leads to dramatic changes in the pH-dependent coordination profile compared to 3G and 2HG (Table 1, Figure 2). The observed spectroscopic changes as well as the proposed complexes (Table 1, Figures 1−3c, and Supporting Information, Figure S6) correspond to those observed for the Cu^{2+} complexes with H-Gly-Gly-His-NH_2[28] (Figure S7a) and H-Gly-Gly-His-OH[27] (Figure S7b). The first complex forms, assigned as CuHL and $CuH_{-1}L$, are observed when pH is increased from 2.5 to 4 (Figure 2c). Unfortunately, low concentrations of the CuHL complex do not allow for the determination of UV−vis and CD spectroscopic parameters of this form. On the basis of the analogy with the H-Gly-Gly-His-OH−Cu^{2+} system it may be proposed that the coordination mode in CuHL is 2N involving the {N_{Im}, NH_2} pair of donors (Supporting Information, Figure S8).[27]

The spectroscopic parameters present in Tables 1 and 4 confirm that the coordination sphere is similar in the cases of $CuH_{-1}L$ and $CuH_{-2}L$, and Cu^{2+} ion is bound by 4N equatorial donor set {N_{Im}, NH_2, $2N^-$} (Figure 7a,b).[27] The formation of $CuH_{-2}L$ complex (Figure 7b) from $CuH_{-1}L$ can be assigned to the loss of a proton from the uncoordinated $-NH_3^+$ group of a second N-terminal branch. However, the mere 0.2 log unit shift for this amino group deprotonation suggests weak interactions.

On the basis of literature reports the UV−vis spectroscopic parameters (λ_{max} = 525 nm, ε = 100 M^{-1} cm^{-1}) for the Cu^{2+} complex of H-Gly-Gly-His-OH (Figure S7b),[27] a similar coordination mode with a 5, 5, 6 chelate pattern can be proposed for $CuH_{-2}L$. On the other hand, the 5, 6, 6 chelate structure with the same donor set in case of the $CuH_{-2}L$ complex, where L = H-Ala-*β*-Ala-His-NH_2 (Figure S7d), leads to λ_{max} = 536 nm and ε = 65 M^{-1} cm^{-1}[28] that further supports the former case, which in turn means the involvement of nitrogen donors at the peptide backbone of 2GH in coordination (Figure 7).

DISCUSSION

A viable strategy to elucidate the metal binding preferences of the branched peptides may be to compare the features of their complexes to those of known peptides representing a specific fragment of the whole molecule. In the structural formula of 3G we can distinguish three domains (Figure 8a,b,c). The first one structurally corresponds to the H-Gly-Gly-Gly-OH peptide

dx.doi.org/10.1021/ic5007428 | Inorg. Chem. 2014, 53, 7951−7959

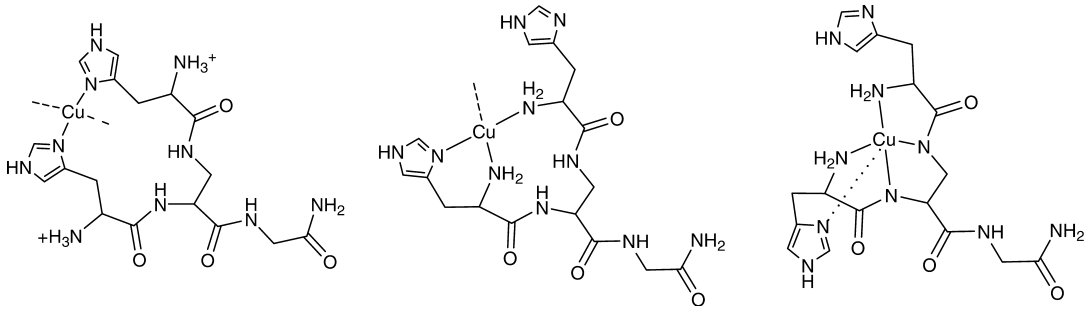

Figure 6. Proposed structures for the major complexes observed in the Cu^{2+}-2HG system. (a) CuH_2L. (b) CuL. (c) $CuH_{-2}L$. The dotted lines (·····) present weak interactions with imidazole donor; discussion provided in text.

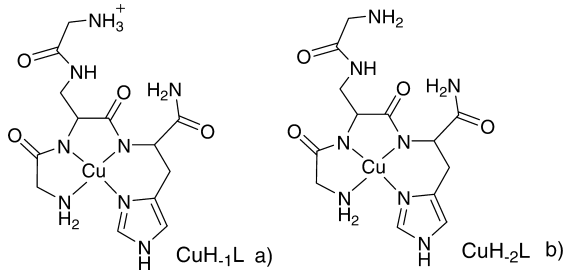

Figure 7. Proposed structure of the major complexes observed in the Cu^{2+}-2GH system: (a) $CuH_{-1}L$ and (b) $CuH_{-2}L$.

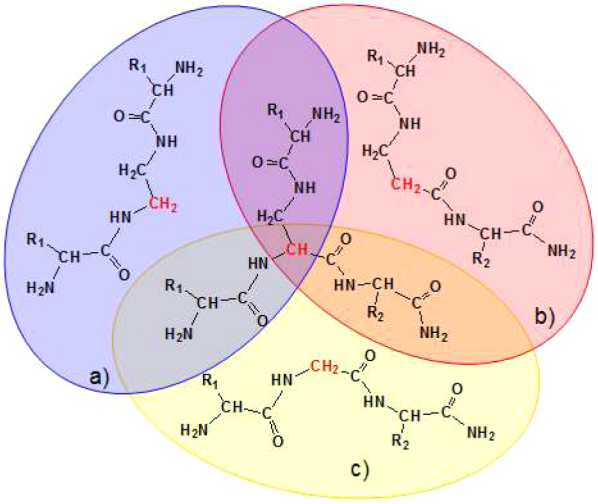

Figure 8. Schematic structural formula for the branched ligands 3G (R_1 = R_2 = H), 2HG (R_1 = 4-methylimidazole, R_2 = H), and 2GH (R_1 = H, R_2 = 4-methyl imidazole) in the center. Linear fragments for comparison: (a) *N*,*N*′-diglycylethane-1,2-diamine (DGEN) when R_1 = H, *N*,*N*′-dihistydylethane-1,2-diamine (DHEN) when R_1 = 4-methylimidazole, (b) H-Gly-*β*-Ala-Gly-NH_2 when R_1 = R_2 = H, (c) H-Gly-Gly-Gly-NH_2 when R_1 = R_2 = H, H-Gly-Gly-His-NH_2 when R_1 = H, R_2 = 4-methylimidazole.

(Supporting Information, Figure S9c), the second to the H-Gly-*β*-Ala-Gly-OH (Figure S9e), and the third to the DGEN or DAEN ligand (Supporting Information, Figure S9b). The Cu^{2+} binding competition between these peptides and 3G shows that $CuH_{-2}L$ is the dominant form in a similar pH range for each system (Supporting Information, Figure S9a). For this reason it is reasonable to compare these complexes. Data indicate that the coordination sphere of $CuH_{-2}L$ form in case of 3G has an equatorial coordination set of $\{2NH_2, 2N^-\}$, making it similar to DGEN[17,19] or DAEN.[18] Interactions of the H-Gly-Gly-Gly-OH and H-Gly-*β*-Ala-Gly-OH-like domains of 3G with Cu^{2+} could not be confirmed. Instead, 3G provides a $\{2NH_2, 2N^-\}$ donor set for Cu^{2+}, whereas for the former domains a $\{NH_2, 2N^-, COO^-\}$ set was confirmed.[29] This indicates that DGEN-like domain of 3G is responsible for the binding of Cu^{2+}. The efficiency of Cu^{2+} binding by 3G is also the highest according to the competition studies (Supporting Information, Figure S9a). These results clearly demonstrate the importance of the branched backbone as a whole in the stabilization of Cu^{2+} complexes compared to the fragments alone.

The extent of the observed stabilization may be attributed in part to the electron-withdrawing effect of the additional peptide bond from the Dap residue, which is not involved directly in the coordination. A similar effect was reported for 4N complexes where the presence of an Asn residue was associated with the lowering of pK_a and the corresponding change in one of the Cu−N bonds.[30,31] Also, secondary interactions may be effective due to the presence of the additional peptide arm, for example, stabilization of the coordinated water molecule via hydrogen bonds.[32]

With respect to the 2HG ligand one can relate the structure to that of *N*,*N*′-dihistydylethane-1,2-diamine (DHEN) (Figure 8a and Supporting Information, Figure S10a). The competition plot (Supporting Information, Figure S10b) between 2HG and reported DHEN complexes[26] shows that 2HG has no overwhelming advantage over its competitor up to pH 8, where the formation of $CuH_{-2}L$ and $CuH_{-3}L$ starts. Seemingly, above this pH the presence of the branched motif in 2HG stabilizes the binding of the Cu^{2+} compared to DHEN. The observed stabilization can be explained by the electronic effect of the branching. Remarkably, such excess stabilization was attributed to the terminal amide moiety in Asn residues,[30,31] an effect that is quantitatively similar to those observed in relation between 3G and DAEN (Supporting Information, Figure S9a). As a result, 2HG will bind Cu^{2+} predominantly over DHEN at pH > ∼ 8.

The Cu^{2+} binding effectivity as a function of pH is different for 2HG and 3G peptides (Figure 9). The competition plot shows that in the pH range of 4−7.5 the Cu^{2+} is bound predominantly by 2HG. This result indicates the effect of histidine on Cu^{2+} binding, which is known for the linear[31,33,34] and cyclic peptides.[35,36] It appears that the presence of histidine results in the ceasing of any interactions between the Cu^{2+} ion and amide donors similarly to linear peptides.[31] At physiological pH, in case of 2HG almost all of Cu^{2+} is bound without the deprotonation of amide donors, whereas in case of 3G almost 90% of copper is bound to $2N^-$ donors. When the pH is increased from 7.5 to 10.5 the difference in Cu^{2+} binding effectivity between 3G and 2HG is lower, roughly 50% of the

dx.doi.org/10.1021/ic5007428 | Inorg. Chem. 2014, 53, 7951−7959

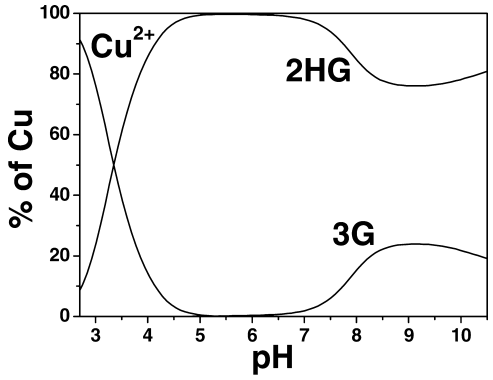

Figure 9. Competition plot for the binding of Cu^{2+} between 2HG and 3G as a function of pH, $[Cu^{2+}] = [2HG] = [3G] = 1 \times 10^{-3}$ M.

Cu^{2+} pool. The complex stabilization in case of 2HG could be assigned to the Cu^{2+} interactions with the imidazole nitrogen of histidine residue, which is consistent with previous findings for $CuH_{-2}L$ complexes with His-Xaa-Xaa linear tripeptides (Xaa = Gly or Ala).[27]

Finally, the competition plot for 1 equiv of Cu^{2+} in the simultaneous presence of equimolar amounts of 3G, 2GH, and 2HG is presented in Figure 10. One can see that the 3G ligand

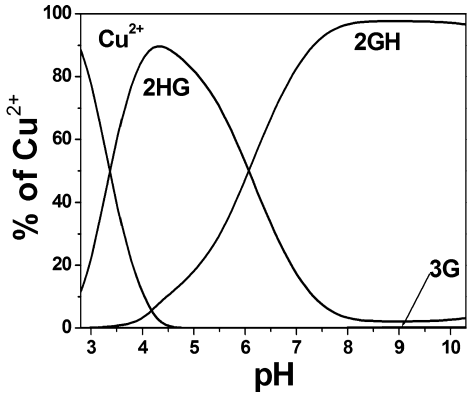

Figure 10. Competition plot for the binding of Cu^{2+} between 3G, 2GH, and 2HG as a function of pH, $[Cu^{2+}] = [3G] = [2GH] = [2HG] = 1 \times 10^{-3}$ M.

cannot be a successful competitor to the histidine-substituted ligands. The Cu^{2+} binding efficiency between 2HG and 2GH is highly dependent on the pH. Up to pH 6 the involvement of both histidine arms of 2HG makes this ligand the dominant copper-binding species, whereas at higher pH the terminal residues of the 2GH main peptide chain (both the C- and N-terminal arms) cannot be matched by 2HG anymore, and binding of Cu^{2+} is most effective in case of 2GH.

It may seem surprising at first glance that the Cu^{2+} chelating affinity order between 2HG and 2GH is switched near the neutral pH. However, literature precedents with the linear domains DHEN and H-GGH-OH—of 2HG and 2GH, respectively—help associate this phenomenon with the location of the histidine residue (see Supporting Information, Figure S11). Additional experimental confirmation could be provided from Figure S12 where we clearly see that at pH 4 UV–vis spectrum of binary Cu^{2+}-2HG system clearly correspond to the ternary system containing Cu^{2+}-2HG-2GH, and at pH 7 we observe that the spectrum of the ternary system matches that of the binary Cu^{2+}-2GH.

CONCLUSIONS

The present study demonstrates that branched peptides based on the Dap central unit show specific properties in the binding of Cu^{2+} ions. For example, both 2GH and 2HG form exceptionally stable complexes with copper leaving one branch free for further functionalization, but the optimal pH range of their highest chelating efficiency is different. This points out that the peptides of such design allow rational modifications in the coordination sphere and creation of complexes with specific complex topology when compared to the linear domains; at the same time, the branches not involved in coordination remain available for other purposes, for example, constructing metallo-dendrimers. This may present a novel approach for tailoring the complex stability or coordination profile and through this, also the enzyme-like catalytic activity. More specifically, the new ligands 3G, 2HG, and 2GH point toward the design of new copper-based models of metallo-enzymes, biosensors and metal-peptide based radiopharmaceuticals.

ASSOCIATED CONTENT

Supporting Information

Structures and spectra (EPR, ESI-MS) of branched peptides, plots of competitive binding according to pH and $\%Cu^{2+}$. This material is available free of charge via the Internet at http://pubs.acs.org.

AUTHOR INFORMATION

Corresponding Author

*E-mail: lukasz.szyrwiel@univ-pau.fr. Phone:(+33)-540 175 037. Fax: (+33)-559 407 681.

Notes

The authors declare no competing financial interest.

ACKNOWLEDGMENTS

This project was financed by Polish Foundation of Science within the POMOST program (POMOST/2012-5/9). Support from the Hungarian Academy of Sciences through a János Bolyai Scholarship is also acknowledged (J.S.P).

REFERENCES

(1) Crespo, L.; Sanclimens, G.; Pons, M.; Giralt, E.; Royo, M.; Albericio, F. *Chem. Rev.* **2005**, *105*, 1663–1682.
(2) Darbre, T.; Reymond, J.-L. *Acc. Chem. Res.* **2006**, *39*, 925–34.
(3) Tam, J. P. *Peptides: Synthesis, Structures, and Applications*; Bern, G., Eds.; Academic Press: San Diego, 1995; pp 455–500.
(4) Welser, K.; Campbell, F.; Kudsiova, L.; Mohammadi, A.; Dawson, N.; Hart, S. L.; Barlow, D. J.; Hailes, H. C.; Lawrence, M. J.; Tabor, A. B. *Mol. Pharmaceutics* **2013**, *10*, 127–41.
(5) Kofoed, J.; Reymond, J.-L. *Curr. Opin. Chem. Biol.* **2005**, *9*, 656–64.
(6) Delort, E.; Nguyen-Trung, N.-Q.; Darbre, T.; Reymond, J.-L. *J. Org. Chem.* **2006**, *71*, 4468–4480.
(7) Bryson, D. I.; Zhang, W.; McLendon, P. M.; Reineke, T. M.; Santos, W. L. *ACS Chem. Biol.* **2011**, *7*, 210–217.
(8) Falciani, C.; Lozzi, L.; Pini, A.; Corti, F.; Fabbrini, M.; Bernini, A.; Lelli, B.; Niccolai, N.; Bracci, L. *Chem. Biol. Drug Des.* **2007**, *69*, 216–221.
(9) Lakatos, A.; Gyurcsik, B.; Nagy, N. V.; Csendes, Z.; Weber, E.; Fulop, L.; Kiss, T. *Dalton Trans.* **2012**, *41*, 1713–1726.
(10) Pettit, L. D.; Pyburn, S.; Bal, W.; Kozlowski, H.; Bataille, M. *J. Chem. Soc., Dalton Trans.* **1990**, 3565–3570.
(11) Jancsó, A.; Selmeczi, K.; Gizzi, P.; Nagy, N. V.; Gajda, T.; Henry, B. *J. Inorg. Biochem.* **2011**, *105*, 92–101.

(12) Sóvágó, I.; Kállay, C.; Várnagy, K. *Coord. Chem. Rev.* **2012**, *256*, 2225−2233.
(13) Stefanowicz, P.; Boratyński, P. J.; Staszewska, A.; Wilczyński, A.; Zimecki, M.; Szewczuk, Z. *Mol. Immunol.* **2004**, *41*, 911−917.
(14) Gans, P.; Sabatini, A.; Vacca, A. *Talanta* **1996**, *43*, 1739−1753.
(15) Neese, F. *QCPE Bulletin;* Indiana University: Bloomington, IN, 1995; Vol. *15*.
(16) Hathaway, B. J.; Wilkinson, G.; Gillard, R. D.; McCleverty, J. A. *Comp. Coord. Chem.* **1987**, *5*, 533−774.
(17) Briellmann, M.; Zuberbühler, A. D. *Helv. Chim. Acta* **1982**, *65*, 46−54.
(18) Armani, E.; Marchelli, R.; Dossena, A.; Casnati, G.; Dallavalle, F. *Helv. Chim. Acta* **1986**, *69*, 1916−1922.
(19) Bai, K. S.; Martell, A. E. *J. Am. Chem. Soc.* **1969**, *91*, 4412−4420.
(20) Lima, L. M. P.; Esteban-Gómez, D.; Delgado, R.; Platas-Iglesias, C.; Tripier, R. *Inorg. Chem.* **2012**, *51*, 6916−6927.
(21) Hathaway, B.; Duggan, M.; Murphy, A.; Mullane, J.; Power, C.; Walsh, A.; Walsh, B. *Coord. Chem. Rev.* **1981**, *36*, 267−324.
(22) Matera-Witkiewicz, A.; Brasuń, J.; Świątek-Kozłowska, J.; Pratesi, A.; Ginanneschi, M.; Messori, L. *J. Inorg. Biochem.* **2009**, *103*, 678−688.
(23) Kállay, C.; Várnagy, K.; Malandrinos, G.; Hadjiliadis, N.; Sanna, D.; Sóvágó, I. *Inorg. Chim. Acta* **2009**, *362*, 935−945.
(24) Lavanant, H.; Virelizier, H.; Hoppilliard, Y. *J. Am. Soc. Mass Spectrom.* **1998**, *9*, 1217−1221.
(25) Prenesti, E.; Daniele, P. G.; Prencipe, M.; Ostacoli, G. *Polyhedron* **1999**, *18*, 3233−3241.
(26) Torok, I.; Gajda, T.; Gyurcsik, B.; K. Toth, G.; Peter, A. *J. Chem. Soc., Dalton Trans.* **1998**, 1205−1212.
(27) Jakab, N. I.; Gyurcsik, B.; Körtvélyesi, T.; Vosekalna, I.; Jensen, J.; Larsen, E. *J. Inorg. Biochem.* **2007**, *101*, 1376−1385.
(28) Nagaj, J.; Stokowa-Sołtys, K.; Zawisza, I.; Jeżowska-Bojczuk, M.; Bonna, A.; Bal, W. *J. Inorg. Biochem.* **2013**, *119*, 85−89.
(29) Sanna, D.; Ágoston, C. G.; Micera, G.; Sóvágó, I. *Polyhedron* **2001**, *20*, 3079−3090.
(30) Bal, W.; Kozlowski, H.; Kupryszewski, G.; Mackiewicz, Z.; Pettit, L.; Robbins, R. *J. Inorg. Biochem.* **1993**, *52*, 79−87.
(31) Kozłowski, H.; Bal, W.; Dyba, M.; Kowalik-Jankowska, T. *Coord. Chem. Rev.* **1999**, *184*, 319−346.
(32) Turi, I.; Sanna, D.; Garribba, E.; Pappalardo, G.; Sóvágó, I. *Polyhedron* **2013**, *62*, 7−17.
(33) Rajkovic, S.; Kallay, C.; Serenyi, R.; Malandrinos, G.; Hadjiliadis, N.; Sanna, D.; Sovago, I. *Dalton Trans.* **2008**, 5059−5071.
(34) Kozłowski, H.; Kowalik-Jankowska, T.; Jeżowska-Bojczuk, M. *Coord. Chem. Rev.* **2005**, *249*, 2323−2334.
(35) Brasun, J.; Gabbiani, C.; Ginanneschi, M.; Messori, L.; Orfei, M.; Swiatek-Kozlowska, J. *J. Inorg. Biochem.* **2004**, *98*, 2016−2021.
(36) Czapor, H.; Bielińska, S.; Kamysz, W.; Szyrwiel, Ł.; Brasuń, J. *J. Inorg. Biochem.* **2011**, *105*, 297−302.

dx.doi.org/10.1021/ic5007428 | *Inorg. Chem.* 2014, 53, 7951−7959